International Journal on Advanced Science Engineering Information Technology

Vol.13 (2023) No. 2
ISSN: 2088-5334

A Study towards a Flapping Robot Maintaining Attitude during Gliding

Muhammad Labiyb Afakh [a,*], Hidaka Sato [a], Naoyuki Takesue [a]

[a] *Department of Mechanical Systems Engineering, Tokyo Metropolitan University, Asahigaoka 6-6, Hino City, 191-0065, Japan*
Corresponding author: [*]afakh-muhammad-labiyb@ed.tmu.ac.jp

***Abstract*— The bio-inspired robot is such a topic that has received growing attention. The ornithopter micro aerial vehicle (MAV) is a challenging topic for bio-inspired robots. This topic combines the research disciplines of Biology, robotics, and aeronautics. Energy efficiency is one of the advantages offered by a flapping robot. Such a flapping robot can glide to perform locomotion to reduce power consumption. We investigated and developed a flapping robot with tail control to maintain the robot's attitude during locomotion/flight, especially gliding. The proposed tail structure mimics an airplane elevator. Lightweight materials and design are considered in this study. The system is designed to allow the robot to have long-range wireless control. The robot can be wirelessly controlled from a base station via a Wi-Fi connection. This study compares a small wing with good stiffness and a large wing with less stiffness. The small wing with good stiffness is better and could generate thrust 1.56 times higher than the large wing. A large wing's leading and trailing edges bending during flapping can be a possible source of induced drag. Gliding performance was also evaluated. The robot could glide up to 8 meters in 2 seconds at 0.9 meters altitude. The developed robot demonstrated an aggressive flight that reached close to 5 m/s. The developed tail mechanism and controller were confirmed that helps the robot maintain its attitude and recover from a stall within a few milliseconds.**

***Keywords*— Bio-inspired robot; flapping robot; ornithopter; tail control; micro aerial vehicle.**

Manuscript received 31 Aug. 2022; revised 23 Sep. 2022; accepted 7 Nov. 2022. Date of publication 30 Apr. 2023.

I. INTRODUCTION

Bio-inspired robots are a growing topic of study. Among bio-inspired robots, the ornithopter micro aerial vehicle (MAV) is one of the more challenging designs. The biology, robotics, and aeronautics disciplines must be blended to achieve an ornithopter due to its complexity and aerodynamic problems. However, flapping robots offer an energy efficiency advantage compared with constantly rotating blades, such as those on drones. To reduce the power consumption, a flapping robot can stop its flapping motion to glide during flight under some circumstances, allowing the wind to flow and push the MAV. An ornithopter produces lift and thrust by flapping its wings, and also uses its main and tail wings to maintain the ornithopter's altitude and attitude. Some researchers have introduced interesting locomotion methods that mimic real birds. Some previous studies [1]–[3] proposed takeoff locomotion that can be a good solution for achieving autonomous flight. Paranjape et al. [4] and Nekoo et al. [5] demonstrated perching locomotion on an ornithopter. That locomotion can be used to save energy and facilitate scouting behavior by being able to perch on a branch. Those capabilities provide enormous potential for application in outdoor environments. Applying an ornithopter to inspect and observe disaster areas is a potential future use. The Fukushima disaster in Japan provides an example situation in which it was dangerous to enter an area. Because these aerial capabilities have been recognized by robotics researchers, they have become a popular topic of study.

One of challenging parts in the development of flapping-wing MAVs is the aerodynamics. Some researchers have conducted the simulations with computational fluid dynamics (CFD) [6]–[9]. Sanuki and Fujikawa [10] analyzed the impact of neutral and flapping angles that influence the attitude during flight. These cause differences in the generated lift and pitch moment. Ding [11] investigated the dynamic performance of a flapping robot under randomly uncertain disturbances. An interesting open-source dynamic simulation was developed by Fei *et al.* [12]. They presented a linear cascading proportional-integral-derivative (PID) control and learning control (reinforcement learning) [13]. OpenAI Gym is also compatible with that simulation.

In general, flapping robots are divided into those for forward flight and hovering [14]. Developing micro- or small-sized hovering robots is possible because the lift vector is the same as the force generated from the flapping motion. Some interesting hovering flapping robots have been extensively studied. Chukewad *et al.* proposed an insect-size flapping robot that can perform locomotion on the water [15]. Ren *et al.* [16] developed a micro-size flapping-wings robot. Tu et al. [17] also studied a hummingbird robot that succeeded in carrying a payload weighing more than 60% of its weight. Fuller [18] introduced a four-wing hovering robot that has steering and payload capacity for autonomy. It can actuate in the yaw axis by moving its wings farther from the center of mass.

Medium- to large-size forward-flight ornithopters are also being developed. Song *et al.* [19] investigated the effects of flapping, twisting, and stretching angles on the wing mechanism. Zhong and Xu [20] studied the power modeling of a large flapping-wing robot. Zuffery *et al.* [21] developed an ornithopter that can carry a payload weighing up to 500 grams. Xu *et al.* [22] proposed a 650 grams ornithopter with a 2.3m wingspan. Their robot, which uses the FreeRTOS system, is capable of autonomous, semi-autonomous, and manually controlled flight.

Sharifzadeh and Aukes [23] experimented with analyzing the buckling of a flapping wing. The results showed that, with the buckling mechanism, the drag could be minimized during the up-stroke. Fan *et al.* [24] suppressed the negative lift and thrust in the upstroke by folding and twisting the wing.

Our first-generation flapping robot, OrnibiBot, could perform takeoff from the ground [3]. In this work, we propose a flapping robot with tail control to stabilize the robot's attitude during gliding and flapping. The tail control also helps the robot to avoid and recover from the stalls. The robot structure easily breaks on impact, so it was built and optimized to simplify assembly and disassembly. Furthermore, we also investigated a small wing with good stiffness and a large wing with less stiffness by conducting force measurement experiments. The result was used to select the main wing structure. Gliding and flight experiments were also conducted to clarify the robot's performance.

This article is organized as follows. Section II introduces the force acting on a flying object, the elevator airplane concept (a tail mechanism), and the developed robot's mechanical structure and control system. Section III reports and discusses the experimental results. The experimental results include force measurement, gliding, aggressive flight, and tail control experiments. The conclusion of the study is given in Section IV.

II. Materials and Method

The aerodynamics, tail mechanism, robot structure, and control system are discussed in this section.

A. Overview of Force Acting on a Flying Object.

In the state-of-the-art development ornithopter, several forces shown in Fig. 1, act on the object's forward flight. Flying animals flap their wings to generate thrust T and lift L to balance the object weight W, which is the mass of the object times the gravitational acceleration. When a flying animal glides, its wings do not produce thrust. Thrust can be produced while the animal descends [25]. Increasing the angle of attack will produce a higher lift, but the angle of attack is limited for flapping robots and other flying objects. A stall may occur if the angle of attack exceeds the limit shown in Fig. 2. To perform a sustainable flight, the following equation must be held.

$$L = W \tag{1}$$

For unaccelerated flight, the generated thrust T from the propulsive mechanism and drag D that is parallel to the relative wind velocity are equal.

$$T = D \tag{2}$$

L and W tend to be larger than T and D for conventional flight situations [26].

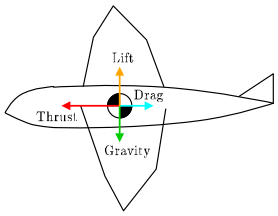

Fig. 1 Force component on a flying object

The center of gravity (COG) can influence the center of aerodynamics (COA) position. The tail will have a greater impact on flight control if the COG is located behind COA. The trade-off is that the flying stability will decrease [27].

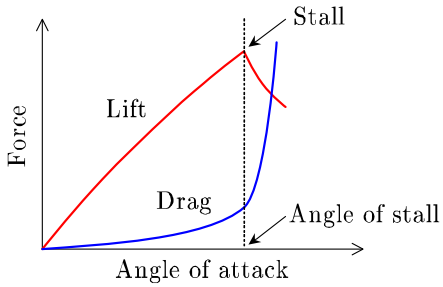

Fig. 2 Lift and drag versus angle of attack

Lightweight designs must be considered to increase the lift-to-weight ratio. The main wing structure, tail wing structure, and COG location also should be considered because they have an enormous impact on robot flight characteristics.

B. Tail Mechanism Based on an Airplane Elevator

The tail mechanism was designed to imitate an airplane elevator, as shown in Fig. 3. Perez-Sanchez *et al.* [28] investigated a morphing tail that uses macro fiber composites. Several tail mechanisms were also compared [29]. The tail is an important component to be studied or optimized because it greatly impacts the behavior of a flapping robot. It helps the robot to increase the generated lift because the attitude of the tail mechanism attitude can change the angle of attack of the robot. A pitch moment is needed for the flapping robot to have a nose-up attitude, which helps the robot to reach higher altitudes. It also helps the robot to perform rolling and pitching motions during flight.

Fig. 3 (a) shows that a pitch moment will be generated when both elevators are in the same position (upward or

downward). Fig. 3 (b) shows that the opposing elevator positions will generate a roll moment, which helps the robot turn left or right. This happens because each tail elevator generates a lift in the opposite direction.

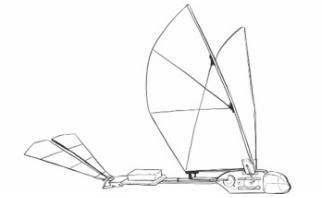

(a) Generating pitch moment.

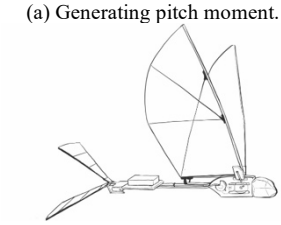

(b) Generating roll moment.

Fig. 3 Tail wing effect according to the tail elevator position

C. Mechanical Structure

The OrnibiBot structure shown in Fig. 4 is divided into three parts: the driving mechanism, wing structure, and tail mechanism. Table I shows the robot specifications. The driving mechanism part modifies the previous robot configuration [3]. It is also closer to and lower concerning the COA. The robot has reduced the drag during flight by making the driving mechanism thinner in the forward-flight axis. The whole robot structure is fabricated to be easy to assemble and disassemble. This is important to be considered because the flapping robot tends to break easily when it falls. To achieve a lightweight structure, fiberglass was selected as the material for the driving system. We have evaluated several materials such as fiberglass, acrylic, and PLA (3D printed part). Acrylic and PLA are lighter weight than fiberglass material, but fiberglass has a good stiffness compared to acrylic and PLA. Since the driving mechanism vibrates a lot, fiberglass is appropriate for the driving mechanism. The wing structure comprises some 3D-printed objects, carbon rods, and ripstop fabric.

Fig. 4 Second-generation OrnibiBot

TABLE I
ROBOT SPECIFICATION

Wingspan	800mm
Input Power	LiPo 3 cells 180mAh
Weight	186 g with battery
Flapping Frequency	8-9 Hz

Fig. 5 shows the implemented driving system, where a three-stage gear reduction increases the generated torque. That gear reduction is needed because the brushless DC (BLDC) motor has less torque. The gear ratio of the driving mechanism can be calculated using Eq. (3).

$$i = \frac{z_2 z_4 z_5}{z_1 z_3 z_6} = \frac{37\times37\times70}{8\times10\times10} \approx 119.8 \quad (3)$$

where z_1, z_2, z_3, z_4, z_5, and z_6 are the number of gear teeth. z_1 is the input shaft gear, which is connected to the BLDC shaft. z_6 is the final gear that transmits the output gear reduction to the output shaft. The wing structure is linked to the output shaft using linkage-rods with ball joints. It converts the rotation in the y-axis to the x-axis, which is the rotation point of the wing hub. Flapping frequency f of the robot can be determined using Eq. (4).

$$f = \frac{\omega}{60i} = \frac{46812\text{rpm}}{60s\times119.8} \approx 9.76\ [\text{Hz}] \quad (4)$$

where ω is the rotation speed of the BLDC motor.

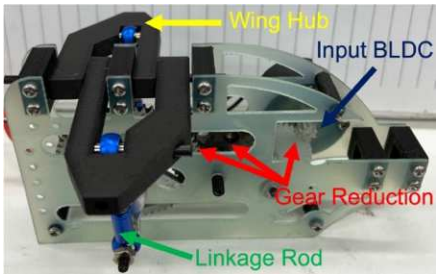

Fig. 5 Driving mechanism

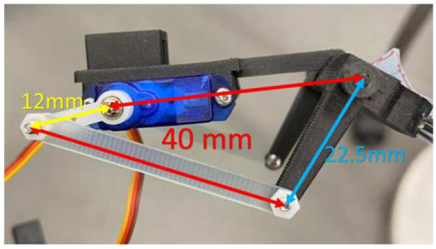

Fig. 6 Tail mechanism

The tail mechanism is illustrated in Fig. 6. Because the tail wing is divided into two pieces, two servo motors are used to actuate the tail wing structure. A crank rocker mechanism inspired this. The output angle θ_o can be calculated using Eq.(5) when the links are parallel.

$$\theta_o = \frac{l_1}{l_2} \cdot \theta_i \quad (5)$$

where θ_i denotes the input angle from the servo motor, l_1 denotes the length of the servo link (12mm), and l_2 is the length of the tail support which (22.5mm).

D. Control Systems

Fig 7 shows an overview of the control system. The OrnibiBot is connected to the base station wirelessly. A low-power single-board computer (Raspberry Pi Zero) and a microcontroller (Arduino Nano 33 BLE Sense) are attached to the robot. The Robotics Operating System (ROS)[30] supports the developed system to govern the robot system and enhance system robustness. A wireless system with a Wi-Fi access point was selected to enable the robot to perform a

long-distance flight. The robot information exchange with the base station is facilitated by using the Raspberry Pi Zero.

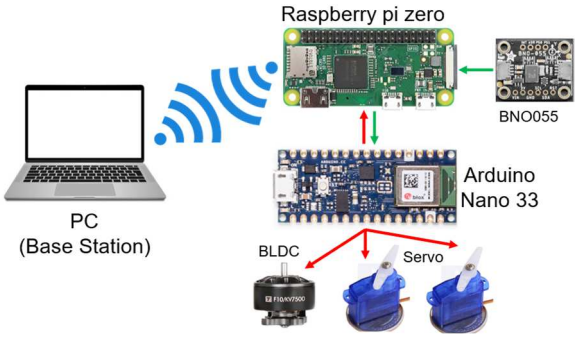

Fig. 7 System Overview

The system also sends commands to the microcontroller to move the actuator via Inter-Integrated Circuit (I2C). The attitude information in roll, pitch, and yaw are gathered from BNO055, which is connected to the single board computer via I2C. The latency of communication via I2C is fast enough to facilitate our system. According to the datasheet of Raspberry Pi Zero and Arduino Nano 33, those allow us to use I2C standard frequency at 100 KHz. The robot transmits those attitude data to the base station during locomotion.

III. Results and Discussion

Several experiments were conducted, as discussed in this section. The first step was to ensure the capability of the flapping robot to fly, and thus a force measurement experiment was conducted.

A. Force Measurement Experiment

The robot was attached to a testing platform. A six-degree-of-freedom force/moment sensor was used to measure the force and moment generated by wing flapping. It is shown in Fig. 8. Fig. 9 shows the manufactured wing structure of the small and the large size.

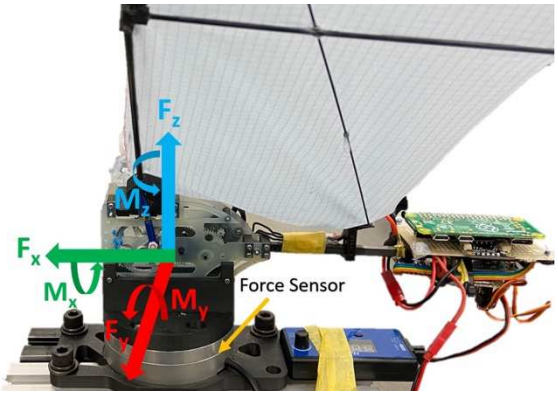

Fig. 8 Testing Platform

The robot flapped for several seconds and recorded the generated force information. Fig. 10 shows the force generated by the small and large flapping-wing structures at a frequency of 8 Hz. Fig. 10 (a) shows the result of the small wing, and (b) shows the result of the large wing. The plots show that the region of the thrust and lift generated by the large-size flapping wing is smaller than the small-size flapping wing.

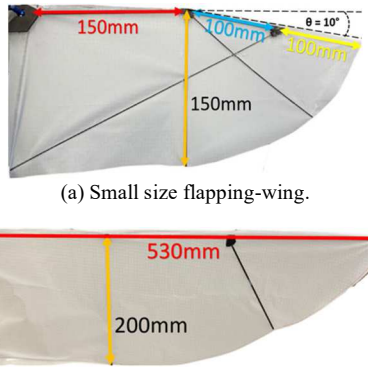

(a) Small size flapping-wing.

(b) Large size flapping-wing.

Fig. 9 Proposed wing structures

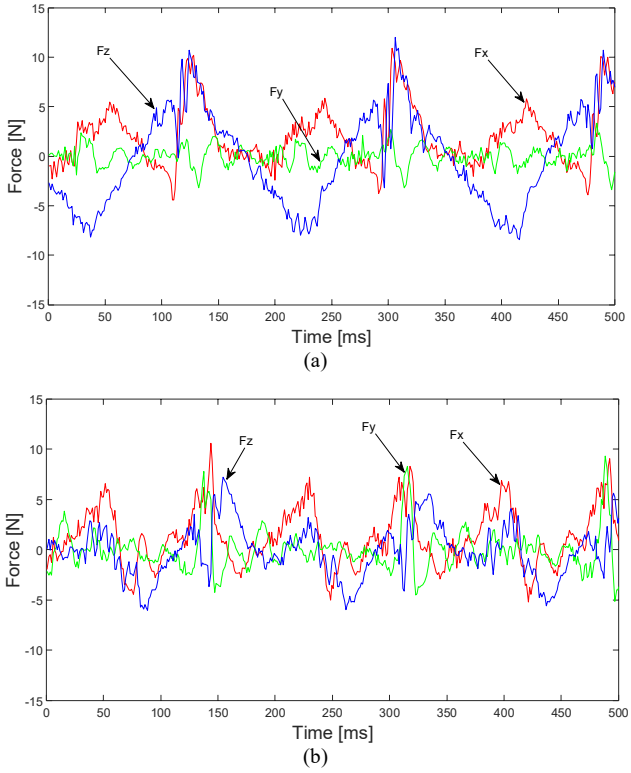

Fig. 10 Measured three-axis force information

TABLE II
AVERAGE AND STANDARD DEVIATION OF FORCES ($\mu \pm \sigma$)

Force	Large Wing Structure	Small Wing Structure
F_x [N]	1.22 ± 2.91	1.91 ± 2.97
F_y [N]	-0.02 ± 2.00	0.02 ± 0.99
F_z [N]	-0.01 ± 2.55	0.05 ± 4.69

Fig. 10 shows the measurement results of the three-axis forces. The measurement details are shown in Table II, which indicates the average and standard deviation of the generated force in three axes. The generated thrust F_x of the small wing, structure is 1.56 times higher than the large wing structure. The average lateral force F_y and lift F_z are nearly equal to zero in both wings. Because the flapping motion originally generates a large deviation, considering the standard deviation can help to determine which wing structure is better. Table II shows that the average lateral force and lift are much smaller than the standard deviation. It can be confirmed that lateral force and lift for both wings are almost zero.

Fig. 11 (a) and (b) show the respective small and large wing bending observed during flapping. The red and blue lines indicate the neutral position of the leading and trailing edges, respectively, and the green line indicates the bending angle of the trailing edge. The results show that the large wing's leading-edge and trailing edge bends easily. The bending angle of the large wing is larger than the small wing. It may induce drag during flapping, so the thrust generated is lower compared to the small wing. It is possible because the large wing structure lacks stiffness. These results indicate that the smaller wing structure with higher stiffness is better than the larger one with less stiffness. Thus, stiffness becomes an important parameter to be considered during designing the flapping wing. Bending will reduce the generated thrust for the FMAVs and induces drag.

(a) Small wing with good stiffness wing.

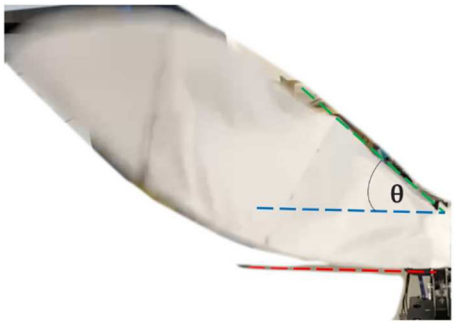

(b) Large wing with a lack of stiffness wing.

Fig. 11 Observation of wing bending

A flat wing structure was selected in the present study, but the NACA airfoil should be considered for gliding efficiency. It may be helpful during the modeling or simulation of the ornithopter. As mentioned in Lang et al. [31]most studies utilize S1223 or modified NACA airfoils as the wing structure. It contrasts with the real bird wing structure. The case of an inclined angle/angle of attack of 0° is not an ideal flapping static force measurement experiment. Several inclined angles are also needed to analyze the coefficient of lift (C_L) and coefficient of thrust according to the inclined angles and flapping frequency.

B. Gliding Experiment

A large area was selected for this experiment, shown in Fig. 12. Fig. 13 shows the gliding experiment, which lasted 1 second. It shows that the robot could glide 5.4 meters at 0.9 meters altitude after launching it by hand. The COG becomes an important property in improving gliding distance. Also, the generation of thrust is needed for gliding. It can be solved by moving the COG forward or descending the angle of attack by setting the tail wing to generate a positive pitch moment.

(a) (b)

Fig. 12 Gliding experiment area. (a) The size of a square tiles and (b) the travel distance for the gliding experiment

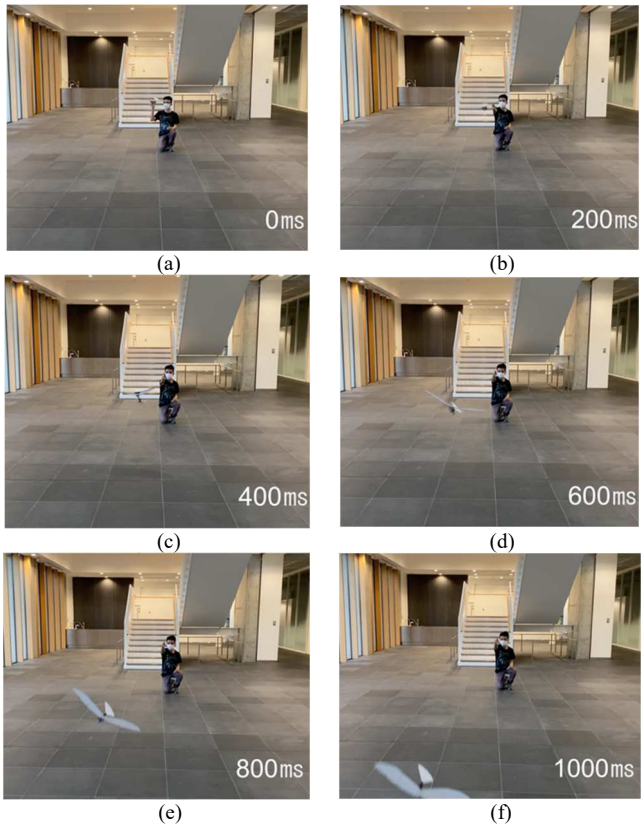

(a) (b) (c) (d) (e) (f)

Fig. 13 Gliding Experiment

C. Flying Experiment.

The flying experiment area is shown in Fig. 14. An investigation of the robot's capability to fly was conducted, as shown in Fig. 15 . It shows that the robot can reached close to 10.2 meters in 2 seconds by setting the actuator rotation speed to 80%. It can be mentioned that the robot achieved ≈ 5.1 m/s for the average velocity assuming the straight-line flight although the robot did not perform a straight-line flight. It becomes a good topic to be developed in the future to control high-speed flight flapping robots. An improved tail structure and mechanism will be considered for the further development to improve navigation robustness. Controlling the position of each wing independently also can be solution to improve navigation, and had been proposed by several researchers [32]–[34].

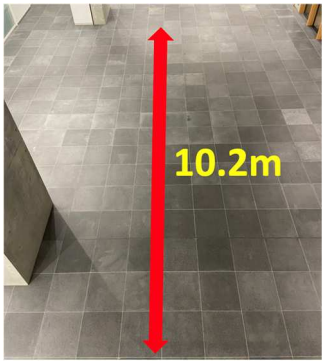

Fig. 14 Flying experiment area

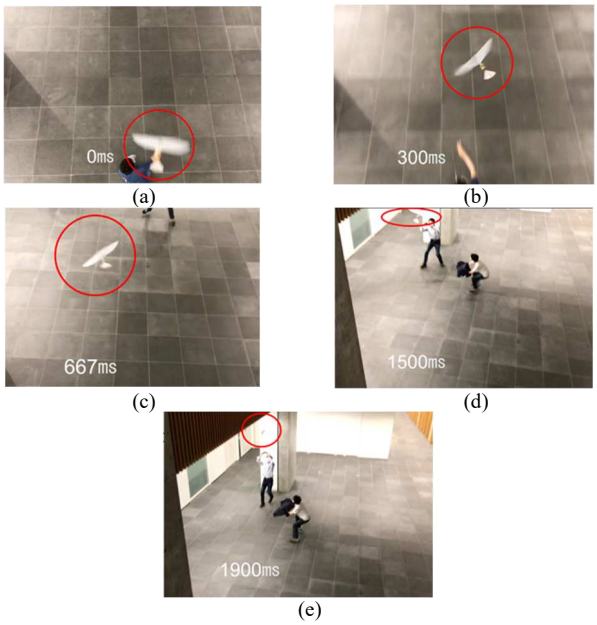

Fig. 15 High speed flapping experiment

D. Tail Control Experiment

Gliding is a unique flight mode that needs to be improved; the robot can stop flapping its wings and reduce energy consumption when the robot glides. However, extending the gliding distance and preventing the robot from stalling is challenging. Thus, we propose that tail control is implemented to help maintain the robot's attitude during gliding. Eq. (6) is the PID controller that is used to control the position of the tail wing according to the attitude information feedback.

$$\mathrm{u}(t) = K_\mathrm{p} e(t) + K_\mathrm{i} \int_0^t e(\tau)\mathrm{d}\tau + K_\mathrm{d} \frac{\mathrm{d}e(t)}{\mathrm{d}t} \qquad (6)$$

where, $\mathrm{u}(t)$ is the command to the tail servo, $e(t)$ is the error of the pitch or roll robot angle against the set point. K_p, K_i, and K_d are the proportional, integral, and derivative gains, respectively [35].

To clarify the effect of tail control, gliding experiment with and without tail control was conducted.

Fig. 16(a) shows the robot's performance without tail control, and (b) shows the performance after tail control was implemented.

Fig. 16 (b) shows that the robot goes through a stall before 2.5 seconds. The rapidly decreasing pitch angle indicates it. The pitch information shows that the robot can recover from the stall in a few milliseconds as the flight time approaches 3 seconds. This good gliding performance is important for the future development of a forward-flight flapping robot. At present, the stability of the robot attitude is not guaranteed because aerodynamics, which greatly affects the stability, is very complex. However, using attitude information in roll and pitch axes to the robot's tail position as feedback information effectively maintained the robot's stability.

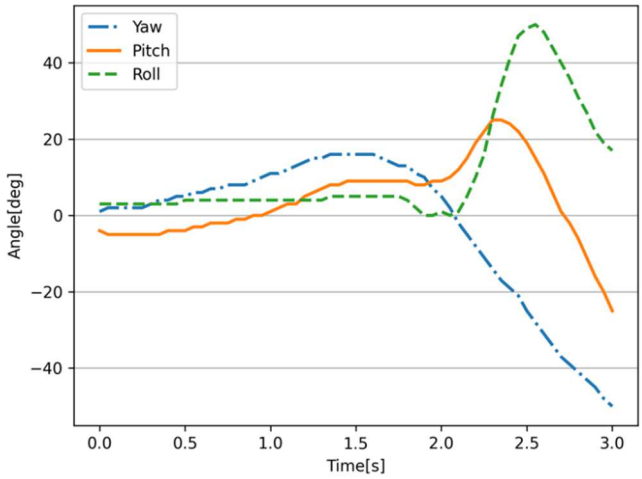

(a) without tail control.

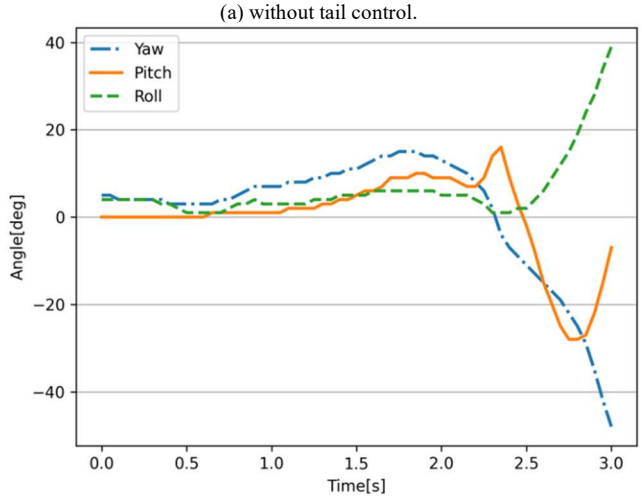

(b) with tail control.

Fig. 16 Robot attitude and stall response during gliding

IV. Conclusion

This study focused on maintaining attitude while gliding towards a flapping robot's development. The COG and COA position were considered to improve the performance. A lightweight structure and less drag are also important considerations for improving performance. Evaluations of small and large wing structures showed that a small wing generated a thrust 1.56 times higher than a large wing. The large wing generates a larger bending angle than the small wing on the leading and trailing edges during flapping because it is comparatively less stiff. This bending may induce drag. To evaluate the performance of the robot, a gliding experiment was conducted. The robot could glide 5.4 meters in 1 second. The robot showed aggressive flight. It could reach an average velocity close to 5.1 m/s. The implementation of tail control by using a PID controller has

succeeded in maintaining the robot's attitude and recovering from a stall.

ACKNOWLEDGMENT

This work was supported by JSPS KAKENHI Grant Number JP21K03965 and TMU local 5G research support.

REFERENCES

[1] J. Zhang, C. Dong, and A. Song, "Jumping aided takeoff: Conceptual design of a bio-inspired jumping-flapping multi-modal locomotion robot," in *2017 IEEE International Conference on Robotics and Biomimetics (ROBIO)*, 2017, pp. 32–37.

[2] S. Yang, Y. Shen, B. Li, Y. Li, and J. Zhang, "Modeling and Simulation of a Flapping-Wing Robot with Active Tails for Balancing Control during Wheeled Running," in *2018 IEEE International Conference on Mechatronics and Automation (ICMA)*, 2018, pp. 1806–1811. doi: 10.1109/ICMA.2018.8484330.

[3] M. L. Afakh, T. Sato, H. Sato, and N. Takesue, "Development of Flapping Robot with Self-Takeoff from The Ground Capability," in *2021 IEEE International Conference on Robotics and Automation (ICRA)*, 2021, pp. 321–327.

[4] A. A. Paranjape, S.-J. Chung, and J. Kim, "Novel Dihedral-Based Control of Flapping-Wing Aircraft With Application to Perching," *IEEE Transactions on Robotics*, vol. 29, no. 5, pp. 1071–1084, Oct. 2013, doi: 10.1109/TRO.2013.2268947.

[5] S. R. Nekoo, D. Feliu-Talegon, J. A. Acosta, and A. Ollero, "A 79.7g Manipulator Prototype for E-Flap Robot: A Plucking-Leaf Application," *IEEE Access*, vol. 10, pp. 65300–65308, Aug. 2022, doi: 10.1109/ACCESS.2022.3184110.

[6] D. Bie, D. Li, J. Xiang, H. Li, Z. Kan, and Y. Sun, "Design, aerodynamic analysis and test flight of a bat-inspired tailless flapping wing unmanned aerial vehicle," *Aerosp Sci Technol*, vol. 112, p. 106557, 2021, doi: https://doi.org/10.1016/j.ast.2021.106557.

[7] G. Arranz, O. Flores, and M. García-Villalba, "Three-dimensional effects on the aerodynamic performance of flapping wings in tandem configuration," *J Fluids Struct*, vol. 94, p. 102893, 2020, doi: https://doi.org/10.1016/j.jfluidstructs.2020.102893.

[8] R. Addo-Akoto, J.-S. Han, and J.-H. Han, "Roles of wing flexibility and kinematics in flapping wing aerodynamics," *J Fluids Struct*, vol. 104, p. 103317, 2021, doi: https://doi.org/10.1016/j.jfluidstructs.2021.103317.

[9] S.-H. Yoon, H. Cho, J. Lee, C. Kim, and S.-J. Shin, "Effects of camber angle on aerodynamic performance of flapping-wing micro air vehicle," *J Fluids Struct*, vol. 97, p. 103101, 2020, doi: https://doi.org/10.1016/j.jfluidstructs.2020.103101.

[10] K. Sanuki and T. Fujikawa, "Motion Analysis of Butterfly-Style Flapping Robot Using CFD Based on 3D-CAD Model and Experimental Flight Data," *Journal of Robotics and Mechatronics*, vol. 33, no. 2, pp. 216–222, 2021, doi: 10.20965/jrm.2021.p0216.

[11] C. Ding, "Dynamic performances of a bird-like flapping wing robot under randomly uncertain disturbances," *PLoS One*, vol. 15, no. 5, pp. e0232202-, May 2020, [Online].

[12] F. Fei, Z. Tu, Y. Yang, J. Zhang, and X. Deng, "Flappy Hummingbird: An Open Source Dynamic Simulation of Flapping Wing Robots and Animals," in *2019 International Conference on Robotics and Automation (ICRA)*, 2019, pp. 9223–9229. doi: 10.1109/ICRA.2019.8794089.

[13] Z. Wang and T. Hong, "Reinforcement learning for building controls: The opportunities and challenges," *Appl Energy*, vol. 269, p. 115036, 2020, doi: https://doi.org/10.1016/j.apenergy.2020.115036.

[14] H. V. Phan and H. C. Park, "Insect-inspired, tailless, hover-capable flapping-wing robots: Recent progress, challenges, and future directions," *Progress in Aerospace Sciences*, vol. 111, p. 100573, 2019, doi: https://doi.org/10.1016/j.paerosci.2019.100573.

[15] Y. M. Chukewad, J. James, A. Singh and S. Fuller, "RoboFly: An Insect-Sized Robot With Simplified Fabrication That Is Capable of Flight, Ground, and Water Surface Locomotion," in *IEEE Transactions on Robotics*, vol. 37, no. 6, pp. 2025-2040, Dec. 2021.

[16] Z. Ren *et al.*, "A High-Lift Micro-Aerial-Robot Powered by Low-Voltage and Long-Endurance Dielectric Elastomer Actuators," *Advanced Materials*, vol. 34, no. 7, p. 2106757, Feb. 2022, doi: https://doi.org/10.1002/adma.202106757.

[17] Z. Tu, F. Fei, J. Zhang, and X. Deng, "An At-Scale Tailless Flapping-Wing Hummingbird Robot. I. Design, Optimization, and Experimental Validation," *IEEE Transactions on Robotics*, vol. 36, no. 5, pp. 1511–1525, 2020, doi: 10.1109/TRO.2020.2993217.

[18] S. B. Fuller, "Four Wings: An Insect-Sized Aerial Robot With Steering Ability and Payload Capacity for Autonomy," *IEEE Robot Autom Lett*, vol. 4, no. 2, pp. 570–577, 2019.

[19] H.-W. Song, Y. Saffar Talori, and J.-S. Zhao, "Bionic Flapping Mechanism of the Wings of a Cursorial Dinosaur Robot for Estimating Its Lift and Thrust," *J Mech Robot*, vol. 13, pp. 1–10, Sep. 2020, doi: 10.1115/1.4048429.

[20] S. Zhong and W. Xu, "Power Modeling and Experiment Study of Large Flapping-Wing Flying Robot during Forward Flight," *Applied Sciences*, vol. 12, no. 6, 2022, doi: 10.3390/app12063176.

[21] R. Zufferey *et al.*, "Design of the High-Payload Flapping Wing Robot E-Flap," *IEEE Robot Autom Lett*, vol. 6, no. 2, pp. 3097–3104, 2021, doi: 10.1109/LRA.2021.3061373.

[22] W. Xu, E. Pan, J. Liu, Y. Li, and H. Yuan, "Flight control of a large-scale flapping-wing flying robotic bird: System development and flight experiment," *Chinese Journal of Aeronautics*, vol. 35, no. 2, pp. 235–249, 2022, doi: https://doi.org/10.1016/j.cja.2021.03.009.

[23] M. Sharifzadeh and D. M. Aukes, "Curvature-Induced Buckling for Flapping-Wing Vehicles," *IEEE/ASME Transactions on Mechatronics*, vol. 26, no. 1, pp. 503–514, 2021.

[24] X. Fan, K. Breuer, and H. Vejdani, "Wing Fold and Twist Greatly Improves Flight Efficiency for Bat-Scale Flapping Wing Robots," in *2021 IEEE/RSJ International Conference on Intelligent Robots and Systems (IROS)*, Sep. 2021, pp. 7391–7397.

[25] W. Shyy, H. Aono, C. Kang, and H. Liu, *An Introduction to Flapping Wing Aerodynamics*. Cambridge: Cambridge University Press, 2013. doi: DOI: 10.1017/CBO9781139583916.

[26] Jr. John D. Anderson, *Fundamentals of aerodynamics*, 5th ed. McGraw-Hill, 2011.

[27] L.-J. Yang and B. Esakki, *Flapping Wing Vehicles: Numerical and Experimental Approach*. 2021. doi: 10.1201/9780429280436.

[28] V. Perez-Sanchez, A. E. Gomez-Tamm, E. Savastano, B. C. Arrue, and A. Ollero, "Bio-Inspired Morphing Tail for Flapping-Wings Aerial Robots Using Macro Fiber Composites," *Applied Sciences*, vol. 11, no. 7, 2021, doi: 10.3390/app11072930.

[29] M. M. Guzmán *et al.*, "Design and comparison of tails for bird-scale flapping-wing robots," in *2021 IEEE/RSJ International Conference on Intelligent Robots and Systems (IROS)*, Sep. 2021, pp. 6358–6365. doi: 10.1109/IROS51168.2021.9635990.

[30] P. Estefo, J. Simmonds, R. Robbes, and J. Fabry, "The Robot Operating System: Package reuse and community dynamics," *Journal of Systems and Software*, vol. 151, pp. 226–242, 2019, doi: https://doi.org/10.1016/j.jss.2019.02.024.

[31] X. Lang, B. Song, W. Yang, and W. Song, "Aerodynamic performance of owl-like airfoil undergoing bio-inspired flapping kinematics," *Chinese Journal of Aeronautics*, vol. 34, no. 5, pp. 239–252, 2021, doi: https://doi.org/10.1016/j.cja.2020.10.017.

[32] H. Sato, M. L. Afakh, and N. Takesue, "Development of Flapping-wing Robot with Independently Controllable Wings," *The Abstracts of the international conference on advanced mechatronics : toward evolutionary fusion of IT and mechatronics : ICAM*, vol. 2021.7, pp. GS6-2-, 2021.

[33] I. Diez-de-los-Rios, A. Suarez, E. Sanchez-Laulhe, I. Armengol, and A. Ollero, "Winged Aerial Robot: Modular Design Approach," in *2021 IEEE International Symposium on Safety, Security, and Rescue Robotics (SSRR)*, 2021, pp. 190–195.

[34] [34] H. Huang, W. He, J. Wang, L. Zhang, and Q. Fu, "An All Servo-Driven Bird-Like Flapping-Wing Aerial Robot Capable of Autonomous Flight," *IEEE/ASME Transactions on Mechatronics*, pp. 1–11, 2022, doi: 10.1109/TMECH.2022.3182418.

[35] R. A. Paz, "The design of the PID controller," *Klipsch school of Electrical and Computer engineering*, vol. 8, pp. 1–23, 2001.